Journal Pre-proof

Metal-Decorated Carbon Nanotubes-Based Sensor Array for Simultaneous Detection of Toxic Gases<!–<ForCover>Icell S, Sara G-Rios, Nashaat A, Miriam A, Xavier V, Nageh KA, Metal-Decorated Carbon Nanotubes-Based Sensor Array for Simultaneous Detection of Toxic Gases, *Journal of Environmental Chemical Engineering*, doi: 10.1016/j.jece.2020.104534</ForCover>–>

Icell Sharafeldin (Data curation) (Formal analysis) (Investigation) (Methodology) (Validation) (Visualization) (Writing - original draft) (Writing - review and editing), Sara Garcia-Rios (Formal analysis) (Investigation) (Methodology) (Validation) (Visualization), Nashaat Ahmed (Formal analysis) (Investigation) (Methodology) (Validation) (Visualization) (Writing - original draft), Miriam Alvarado (Formal analysis) (Investigation) (Methodology) (Validation) (Visualization), Xavier Vilanova (Investigation) (Resources) (Supervision) (Writing - original draft) (Writing - review and editing), Nageh K. Allam (Conceptualization) (Formal analysis) (Funding acquisition) (Project administration) (Resources) (Supervision) (Visualization) (Writing - original draft) (Writing - review and editing)

PII:	S2213-3437(20)30883-6
DOI:	https://doi.org/10.1016/j.jece.2020.104534
Reference:	JECE 104534
To appear in:	*Journal of Environmental Chemical Engineering*
Received Date:	15 May 2020
Revised Date:	26 August 2020
Accepted Date:	20 September 2020

Please cite this article as: { doi: https://doi.org/

Metal-Decorated Carbon Nanotubes-Based Sensor Array for Simultaneous Detection of Toxic Gases

Icell Sharafeldin[1], Sara Garcia-Rios[2], Nashaat Ahmed[1], Miriam Alvarado [2], Xavier Vilanova[2], Nageh K. Allam[1, *]

[1]Energy Materials Laboratory, School of Sciences and Engineering, The American University in Cairo, New Cairo 11835, Egypt

[2]Departament d'Enginyeria Electrònica, Escola Tècnica Superior d'Enginyeria, Universitat Rovira i Virgili, Avda. Països Catalans 26, 43007 Tarragona, Spain

* Corresponding Author E-mail: nageh.allam@aucegypt.edu

Graphical abstract

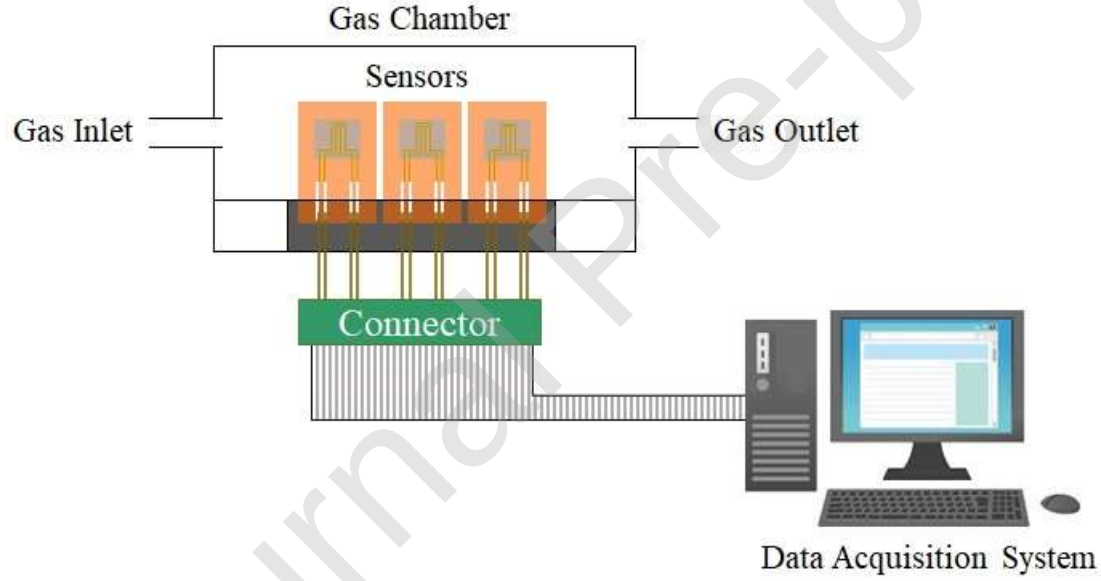

Research Highlights

1. Metal-decorated carbon nanotubes-based sensor arrays were successfully fabricated.
2. CO and NO_2 exposure showed the lowest and highest overall resistance change.
3. Cu-decorated CNTs showed the highest resistance change response to H_2S gas.
4. NH_3 showed the highest response to Ru-decorated CNTs.
5. DFT calculations enabled the in-depth understanding of the electron transfer mechanism.

Abstract

Herein, we report a toxic gas detector based on an array of metal-decorated multiwalled carbon nanotubes (M-MWCNTs) sensors. The room temperature (20°C) response of the sensors array towards NO_2, H_2S, NH_3, and CO gases was investigated. The MWCNTs were decorated with transition metals, Pt, Ti, Ag, Ru, and Cu to enhance the sensitivity and selectivity of the carbon nanotubes to the toxic gases. The M-MWCNTs powders were deposited on gold electrodes and printed on flexible Kapton sheets to form the sensors array. CO exhibited the lowest resistance change response for all six sensors (five transition metal-decorated MWCNTs sensors and one pristine MWCNTs-based sensor), with the Ag-MWCNTs sensor exhibiting the highest response of 0.047 to 100 ppm CO. The Ag-MWCNTs also revealed the relatively highest sensitivity of 0.944 upon exposure to 100 ppm NH_3. The Cu-MWCNTs sensor showed the highest sensitivity of 1.75 upon exposure to 10 ppm H_2S, while the Pt-MWCNTs sensor showed the highest response of 1.96 upon exposure to 10 ppm NO_2. A unique response pattern was generated for each gas that can be used for its identification. The experimental results were also compared to our previously reported density functional theory (DFT) calculations, revealing the same order of resistance change, thereby validating the use of DFT as a tool to predict the interaction properties and providing an in-depth understanding of the reducing/oxidizing gas electron transfer mechanisms.

Keywords*:* gas sensor; carbon nanotubes; transition metal decoration.

1. Introduction

Gas sensing methods are essential in several vital applications such as environmental monitoring; breath analysers for medical diagnosis; chemical and polymer manufacturing; and natural gas detection in petroleum engineering applications. Moreover, the 2019 "Gas Sensors Market Size, Share, System and Industry Analysis and Market Forecast to 2024" report published by Markets and Markets™ estimates a projected growth of the gas sensors market size from USD 1.0 billion in 2019 to USD 1.4 billion by 2024 [1]. Currently, metal oxide sensors based on both single- (e.g., ZnO, SnO_2, WO_3, TiO_2, and Fe_2O_3) and multi-component oxides ($BiFeO_3$, $MgAl_2O_4$ and $SrTiO_3$) [2] are the widely used choice for a range of gasess due to their low cost and simplicity [3]. Researchers are investigating numerous alternatives for gas sensing catalysts including metal oxides [4,5], perovskites [6], metal-organic frameworks [7,8],

imprinted polymers [9], carbon nanomaterials [10], quantum dots [11], and nano/mesoporous materials [12]. For polymers, the reduction of the electrical percolation threshold of conductive polymer composites can be achieved by using conductive fillers with a large aspect ratio (or surface area) such as carbon nanotubes (CNTs). At the percolation threshold filler concentration, the filler starts to form an electrically conductive network and when exposed to the target gas, the conductive network changes its structure with the resulting electrical resistance change is the measuring signal in vapor sensing [13]. Nano/mesoporous materials, such as 2D metallic iridium (Ir), exhibit a high electrocatalytic activity toward oxygen evolution reaction (OER) [12]. Tuning the properties of the structure, such as the orientation of the channel structure, the composition, and the porosity, enhances the gas sensitivity and significantly improves the oxygen evolution reaction (OER) [14]. By selecting the appropriate surfactants or block copolymers and solvent compositions [15], the properties of the porous structure can be tuned.

Carbon nanotubes have several advantages as active sensing materials including a high surface-area-to-volume ratio, high carrier mobility, and the ability to operate at room temperature [16,17]. However, CNTs suffer from weak binding energy and minor charge transfer between their surfaces and the adsorbed gas molecules [18]. Researchers are investigating the functionalization and decoration of the carbon nanotube walls to enhance the catalytic activity and response of carbon nanotubes to the targeted gases. Presently, non-noble metal and nitrogen co-doped carbon materials are promising catalysts to replace Pt-based catalysts toward ORR, such as typical iron and nitrogen co-doped carbon materials [19]. Verissimo et al. synthesised single/multi-walled carbon nanotubes (SWCNTs/MWCNTs) decorated with cerium-praseodymium oxide nanoparticles (CePr-oxides) [20]. The CePr-oxides exhibited an enhanced sensitivity towards 10 ppm H_2S gas sensing at room temperature [20]. Angjellari et al. found that the sensitivity to 1% NH_3 gas of SWCNTs increased from 1.58 to 5.87 when the SWCNTs were decorated with nickel. SWCNTs [21], in this case, are a p-type conductor and when exposed to the electron-donating ammonia gas, they gain electrons, thereby decreasing their main current carrier concentration and increasing their resistance. The addition of nickel causes their d-orbitals to take part in the electron donation from ammonia to the SWCNTs and increases the number of ammonia molecules adsorbed on

the surface, making the material more sensitive [21]. Also, for MWCNTs, Espinosa et al. [22] studied the response of oxide-functionalised MWCNTs to NO_2 and CO gases. They deposited SnO_2, WO_3 or TiO_2 sensing layers such that they became embedded inside the oxygen-functionalised MWCNTs. The highest sensitivity achieved for NO_2 was 0.51 at 25°C for SnO_2/MWCNTs and 0.14 at 150°C for WO_3/MWCNTs for CO sensing. They found that the sensors' responsiveness heavily depended on the quantity of MWCNTs dispersed on the metal oxide matrix. Moreover, the SnO_2 or WO_3 films are n-type semiconductors while the oxygen-functionalised MWCNTs films behave as p-type semiconductors; layering the metal-oxide decorated films and the oxygen-functionalised MWCNT films result in the formation of p-n junctions at the interface which enhanced the conductivity of electrons when exposed to the target gas [22]. Penza et al. demonstrated another mechanism for improving the charge transfer, i.e. sensitivity of the active material. They examined the difference in sensitivity between unmodified and Pt- and Au-modified MWCNTs sensors and found that the functionalised MWCNTs exhibited higher gas sensitivity up to (6x-8x) and (2x-3x) for NH_3 and NO_2, respectively, at sensor temperatures of 100–250°C [23]. This improvement in sensitivity is due to the effect of direct charge injection and catalytically induced charge into functionalised MWCNTs [24]. Star et al. investigated the differences in the catalytic activity of 18 catalytic metals decorated on carbon nanotube field-effect transistor for the detection of H_2, CH_4, CO, and H_2S gases [25]. A sensor array, fabricated by site-selective electroplating of Pd, Pt, Rh, and Au metals, demonstrated improved sensitivity towards the gases [25]. Those studies clearly demonstrate that functionalization significantly improves the sensitivity of carbon nanotubes to the targeted gases. The sensitivity depends on the charge transfer mechanism, which depends on the structure and nature of the gas as well as surface interactions. Transition metals, in particular, offer a great potential as dopants to improve catalysis [26]. The unique d electronic configuration and spectral characteristics of transition metals allow the insertion of new bands in the semiconductor band gap and/or modify the conduction band (CB) or valence band (VB) positions [27].

Herein, we aim at the demonstration of a novel approach to the design of a sensor array based on different metal-decorated CNTs using simple MWCNTs decoration techniques coupled with room

temperature operation and sensors based on flexible gold-printed electrodes. Moreover, we aim to define a unique response pattern constructed by the combination of the different metal-decorated MWCNTs sensors to enhance the selectivity of the detector. For this work, we chose to start with investigating Cu, Pt, Ti, Ru and Ag as the carbon nanotube decorations and to test the fabricated sensors to four target gases; CO, NH_3, NO_2, and H_2S on account of their hazardous effects on the environment and human health. Moreover, a comparison of the experimental findings to our previously reported DFT calculations [28] was introduced and discussed, revealing the advantage of DFT calculations in providing a deeper insight into the adsorption mechanism between the gas molecule and the carbon nanotube surface as well as successfully predicting the order of the resistance change responses.

2. Methodology

2.1. Synthesis of M-MWCNTs

MWCNTs were purchased from *NanoTech Egypt for Photoelectronics*, with an average size of 660 nm in length and 20 ± 5 nm in diameter. To decorate the carbon nanotubes with metals, a total solute weight of 0.05 g was maintained for all samples comprised of 0.045 g of carbon nanotubes and 0.005 g of the desired decoration metal. The following metal salts and compounds were used: Titanium (IV) isopropoxide: Alfa Aesar, 97+%, Liquid, $Ti[OCH(CH_3)_2]_4$, ThermoFisher (Kandel) GmbH, Germany. Silver nitrate: Alfa Aesar, 99+%, $AgNO_3$, ThermoFisher (Kandel) GmbH, Germany. Copper (II) chloride: Sigma Aldrich, $CuCl_2$, powder 99%. Ruthenium (III) chloride hydrate: Alfa Aesar, 99.9+%, $Cl_3Ru•xH_2O$, ThermoFisher (Kandel) GmbH, Germany. Chloroplatinic acid hexahydrate: Sigma Aldrich, $H_2PtCl_6•6H_2O$, CS reagent ≥ 37.50% Pt basis. To achieve 0.005 g of the desired metal, the following masses of the salts were used, based on their molecular masses: 0.0297 g of $Ti[OCH(CH_3)_2]_4$, 0.00787 g of $AgNO_3$, 0.01057 g of $CuCl_2$, 0.0102 g of $RuCl_3$, and 0.0133 g of $_2PtCl_6•6H_2O$. The salts (or liquid in the case of Titanium (IV) isopropoxide) and 0.045 g of the multiwall carbon nanotubes were added to 80 ml ethanol mixture. The mixture was sonicated for 20 minutes to ensure thorough dispersion, then

placed in an autoclave (in air) and heated at 180°C for 10 h, after which the mixture was filtered, centrifuged, and dried in the oven at 60° C for 12 h.

2.2. Sensor Fabrication

The M-MWCNTs were deposited over flexible Kapton® HPP-ST (2 mil) substrates with inkjet-printing electrodes. The electrodes were made of gold ink (NPG-J, Harima Chemicals Inc.) and printed through a Dimatix Materials Printer DMP-2850 (Fujifilm Dimatix Inc., Santa Clara, CA). The design of the electrodes consisted of a pair of parallel electrodes and a coplanar heater. The inner 'legs' are designed to measure the resistance and the outer 'legs' of the electrode are used to add external heating if required **(Figure 1a)**. The heater was not used in our case as this experiment consisted of testing the gas response at room temperature. The tracks of the electrodes had a width of 170 μm and the gap between electrodes was 140 μm. The gold tracks are easily scratched by contact with the connector of the sensing chamber therefore, silver contact pads were painted at the end of the gold tracks to prevent damage. A Kapton mask, in the shape of the contact pads, was used to deposit silver ink (DuPont 5064H) then, the silver ink was dried in an oven for 30 min at 130°C **(Figure 1b)**. To define the deposition of the M-MWCNTs area, a Kapton mask with a square opening of 5 mm x 5 mm was placed over the electrodes **(Figure 1c)** and the set-up was placed over a hot-plate to deposit the MWCNTs **(Figure 1d)**. The temperature of the hot-plate was set at 100°C. The MWCNTs were dispersed in ethanol (96%, Scharlau) and sonicated for 1 h to ensure homogenous dispersion. Afterwards, an airbrush was filled with 2 ml of the MWCNT dispersion and the solution was sprayed over the substrate. Finally, the sensors were kept over the hot-plate until dry the layer **(Figure 1d)**. The sensor could not be weighed before and after M-MWCNTs deposition to quantify the amount of M-MWCNTs deposited on the surface using the airbrushing technique because the difference in weight of the M-MWCNTs would have been negligible compared to the weight of the Kapton sensor. Thus, we relied on the electrical resistance measurement of the M-MWCNTs to ensure that a similar amount of M-MWCNTs deposition occurred for the different M-MWCNTs. The higher the resistance measured indicates a higher amount of M-MWCNTs. The initial resistance (in ambient air) was

measured and found that they were all in the similar range of 200-400 Ω, which is acceptable. A total number of 6 sensors were prepared: Ru-Decorated MWCNTs, Pt-Decorated MWCNTs and Ti-Decorated MWCNTs shown in **Figure 1e**, and Cu-Decorated MWCNTs, Ag-Decorated MWCNTs, and Pristine MWCNTs.

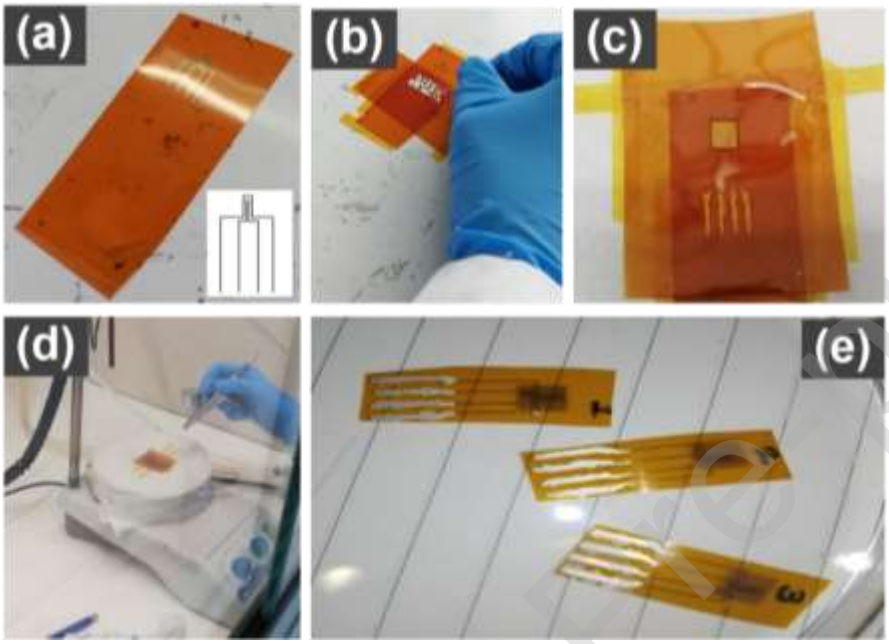

Figure 1: Photos of the different stages on the sensor fabrication process. **a.** The gold-printed electrodes on Kapton sheet. ***Inset:*** Schematic of the gold printed electrodes. **b.** Overlaying the mask for the contacts and painting the silver contacts. **c.** Overlaying the square mask for the M-MWCNT deposition over the sensor. **d.** Placing the sensor plus square mask on a hotplate and airbrushing the M-MWCNT solution over the square mask. **e.** The completed sensors: (1) Ru-MWCNT, (2) Pt-MWCNT, and (3) Ti-MWCNT. The rectangular Kapton sheet, with the 4 printed gold electrodes in contact with the 4 silver contacts. The darker grey square on top of the gold contacts is the deposited M-MWCNTs material.

2.3. Sensor Testing

The fabricated sensors were placed in a connector inside a 20 cm^3 Teflon chamber. The schematic of the testing system used is presented in **Figure 2**. Approximately 2 h of synthetic dry air (Air Premier Purity: 99.995 %) was first passed through the chamber to stabilize the sensor resistance. The resistance measurements were performed using a data acquisition unit (Agilent 34970A). The script was set to run 2 h of synthetic air followed by 20 min of the target gas and then another 1 h of synthetic dry air. This script is then set to repeat four times giving us a total of 4 pulses of the target gas, i.e. four opportunities for the

gas to induce a change in the active material with 3 h of synthetic air between pulses to allow for sensor recovery. Each type of M-MWCNTs powder was deposited on one sensor, giving a total of 6 sensors. Each sensor was tested 3 times for each gas, giving a total of 12 runs. In each run, the response to the gas was tested with 4 pulses giving a total of 48 pulses. We used simple average statistical methods to derive the final response.

The flow rate for the synthetic air and target gases was set at 100 sccm (standardized cubic centimetre). The target gases and their concentrations tested were CO=100 ppm, NO_2=10 ppm, H_2S=10 ppm and NH_3=100 ppm. The concentrations of the target gases were kept constant at these values throughout the experiment. The testing temperature was also kept constant at 20°C throughout the experiment. The gas concentrations were controlled via PC by a set of mass flows (Bronkhost Hitech 7.03.241). The gas concentrations were obtained by diluting the target gas with synthetic dry air when needed. For example, the CO cylinder was 100 ppm from the manufacturer, so this was not diluted in synthetic air and was supplied 100% directly from the cylinder and was measured by the flow meter. The NO_2 cylinder, on the other hand, was 100 ppm from the manufacturer and the target concentration was 10 ppm so we diluted 10% of the flow from the NO_2 cylinder with 90% synthetic air to achieve the target 10 ppm concentration of NO_2.

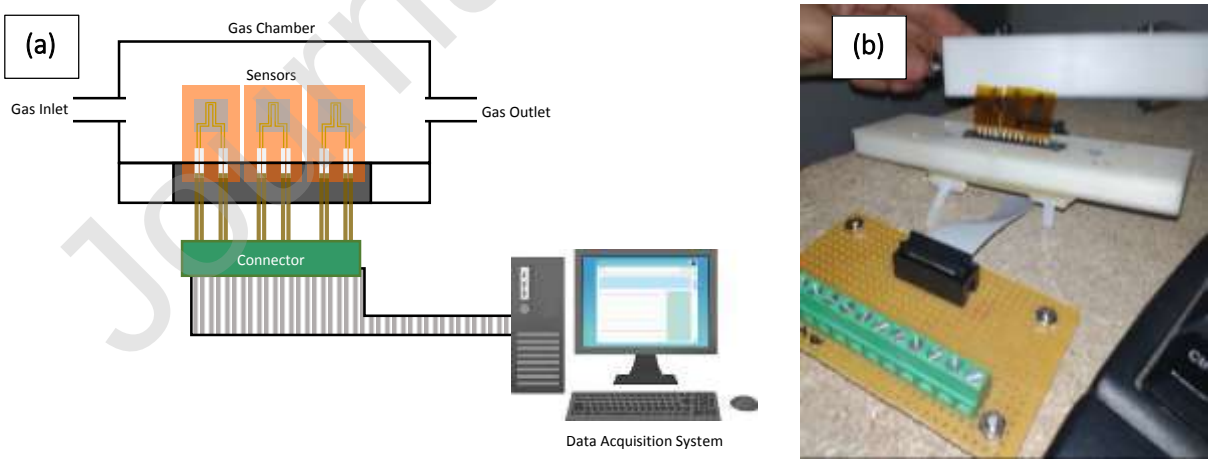

Figure 2: Testing System Schematic **(a)** and Photo **(b)**: The sensors were placed in a connector inside a Teflon chamber which is securely fastened and only allows for the gas to travel through the inlet and outlet. The data acquisition system reads the resistance changes through the connector.

3. Results

3.1. Characterisation

Energy Dispersive X-ray (EDX) analysis of each of the metal-decorated carbon nanotube samples was performed using the JEOL JED-2300 Analysis Station plus. The EDX analysis was used to determine the weight percentage loading of each metal. The EDX analysis showed that the average weight percentage of the metals compared to carbon were 12.36%, 10.97%, 13.01%, 4.26% and 6.56% for Pt, Ru, Ti, Ag and Cu decorated MWCNTs, respectively **(Figure 3ai)**. A detailed table presenting the weight% of three samples of each M-MWCNT and their average is included in the supplementary information, **Table S1**. Transmission Electron Microscopy (TEM) images of the pristine and synthesized M-MWCNT powders were taken using JOEL JEM 2100 ultra-high-resolution analytical electron microscope **(Figures 3aii-3fii)** and show the formation of clusters attached to the walls of the carbon nanotubes. Size analysis of the TEM images showed that the formed Pt clusters were larger than the Ru counterparts, reaching 13.15 to 18.63 nm in diameter, while in the case of Ru, the average size of the clusters formed ranged from 4.25 nm to 6.67 nm in diameter. The average size of the Ti cluster diameter was 11.24 nm. The size of the formed Ag clusters ranged from 13.03 to 16.89 nm in diameter. The EDX analysis of the Cu-decorated MWCNTs showed an average wt% of 6.56 of Cu compared to 93.44 wt% carbon. The TEM images revealed that copper appears as flakes surrounding the carbon nanotubes. Copper may have been deposited as flakes instead of clusters due to the possible oxidation of copper. Copper flakes ranged in size from 50.55 nm to approximately 92.81 nm in width. Note that the synthesis method allowed for loading of very close wt% of the metals, thereby limiting the number of variables affecting resistance change for analysis of the sensors.

Raman analysis was conducted using Raman FT-IR spectrometer, Renishaw Confocal microscopy Leica DM 2500 FT-IR IluminatIR II, Smith Streamline Raman Imaging. Raman analysis was used to ensure that the synthesis method resulted in effective metal decoration of the carbon nanotube walls through defect formation by observing the changes in the peaks of the Raman spectra. **Figure 4**

presents the Raman spectra of each of the M-MWCNTs as well as the pristine MWCNTs. The standard Raman spectra for multiwalled carbon nanotubes is characterised by the occurrence of the D-band at 1345 cm^{-1} and G-band at 1576 cm^{-1}. The D-band corresponds to the sp^3-hybridized, diamond-like carbon bonds i.e. the degree of nanotubes structure disorder, which can be ascribed to impurities and/or lattice distortions due to nanotubes bending, finite size of crystalline domains, and existing functional groups created during purification with acid or created by oxidation [29]. The G band is the characteristic peak for all sp^2 hybridized carbon allotropes [29] i.e. the degree of nanotube graphitization. This, and 2D-band at 2685 cm^{-1} corresponding to stresses and the lack of presence of the Radial Breathing Mode band [30].

During the oxidation treatment of graphitic structures, oxygenated functional groups can form, which change the atomic structure of carbon atoms from C-C sp^2 to C-C sp^3. Also, the oxidation treatment can remove the remaining amorphous carbon (C-C sp^3) [31]. The intensity ratio of the D-to-G bands (I_D/I_G) is commonly used to evaluate the disorder degree of graphitic materials [32]. An increase in I_D/I_G suggests a decrease in the average size of C-C sp^2 domains caused by the increase of oxygen functional groups attached to the MWCNTs wall to be greater than the oxidation of the amorphous carbon of the nanotube walls [33].

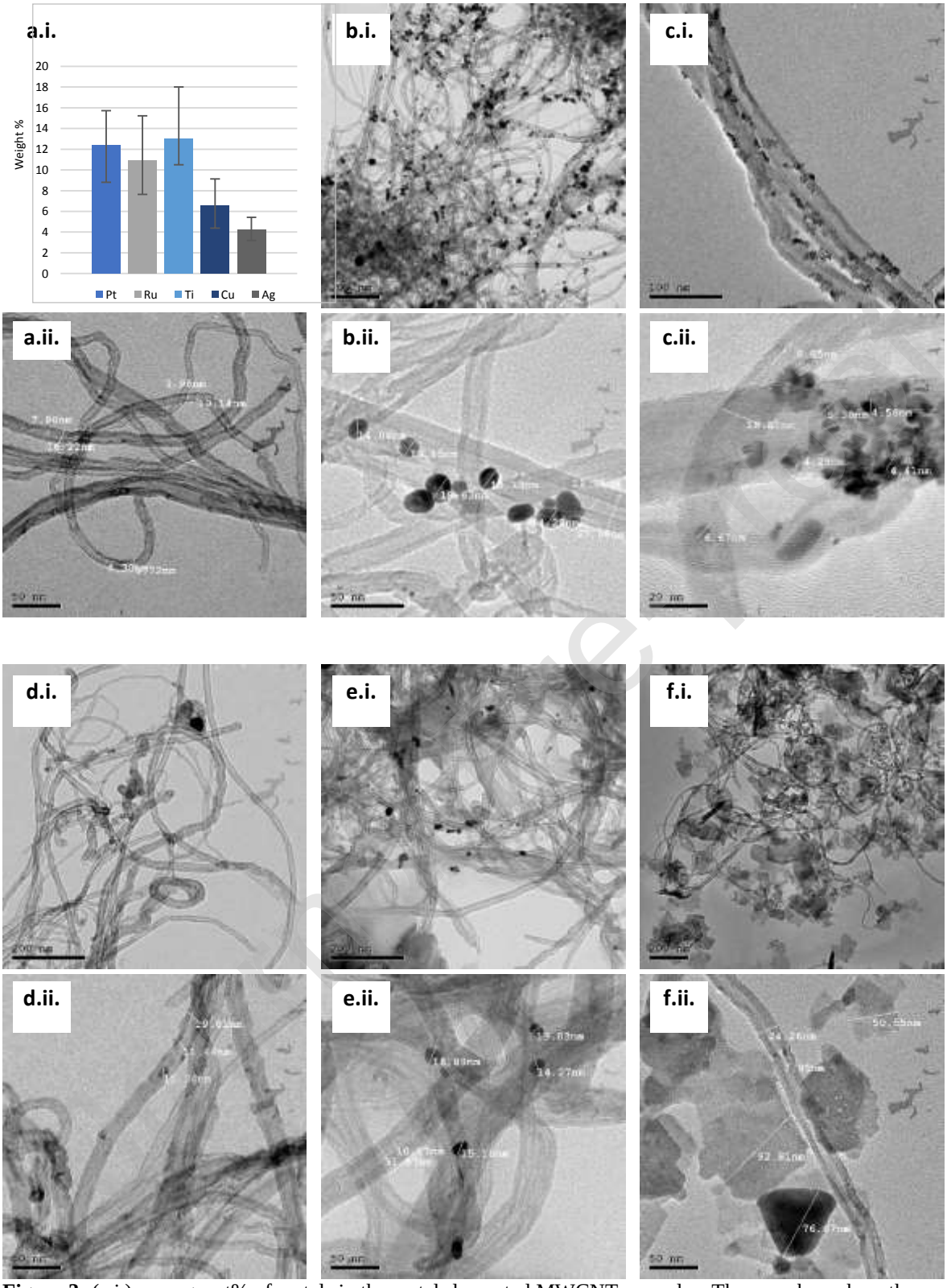

Figure 3: (a.i.) average wt% of metals in the metal-decorated MWCNTs samples. The error bars show the range of wt% out of the 3 samples tested. TEM images of pristine MWCNT (a.ii.) and decorated MWCNTs with measurements of metal clusters. (b.i. and b.ii.) Pt-MWCNTs, (c.i. and c.ii.) Ru-MWCNTs, (d.i. and d.ii.) Ti-MWCNTs, (e.i. and e.ii.) Ag-MWCNTs and (f.i. and f.ii.) Cu-MWCNTs.

The values of I_D/I_G of pristine MWCNTs and metal-decorated MWCNTs have been calculated as shown in **Table 1**. The I_D/I_G ratio for the M-MWCNTs is higher than that of the pristine counterpart. The increase in the I_D/I_G ratio after decoration indicates the attachment of metal nanocluster functional groups onto the surface of the carbon nanotubes, thereby creating defect sites [29]. The I_D/I_G values for all the M-MWCNTs fall within the same range of 0.9-1.0, with the Cu and Ag decorations having the lowest defects of 0.91 and 0.92 followed by Pt and Ti at 0.95 and 0.94 I_D/I_G ratio and the highest is observed for Ru decoration at 1.01 I_D/I_G ratio, i.e. the highest defects. The similar I_D/I_G range 0.9-1.01indicates that the synthesis method was successful in creating an equal and fair dopant metal percentage for all metals.

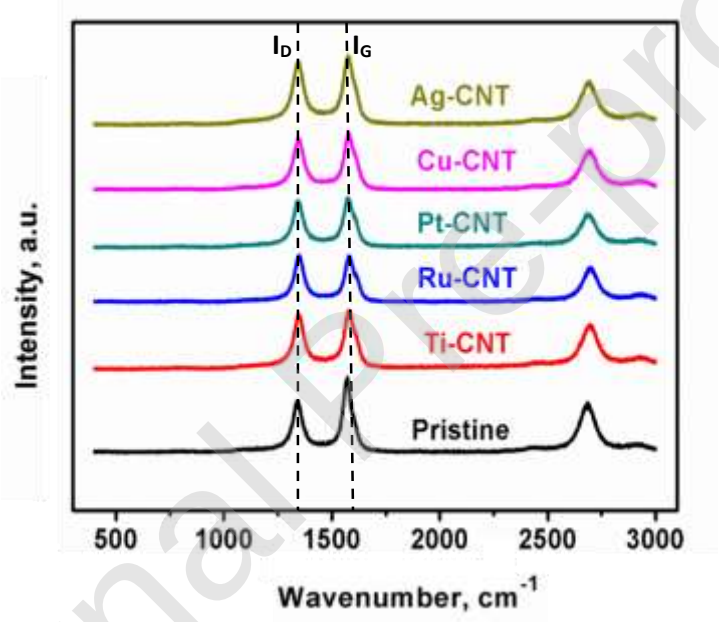

Figure 4: Raman spectra of the synthesized metal-decorated carbon nanotubes.

Table 1: Summary of the Raman analysis of the fabricated M-MWCNTs

Material	**I_D**	**I_G**	**I_D/I_G**
Pristine MWCNT	2540	3630	0.70
Ti-MWCNT	2750	2930	0.94
Ru-MWCNT	2290	2270	1.01
Pt-MWCNT	2365	2500	0.95
Cu-MWCNT	2510	2770	0.91
Ag-MWCNT	3120	3380	0.92

Therefore, the EDX, TEM and Raman analyses indicate that the synthesis method was successful in producing metal clusters attached to the walls of the multiwall carbon nanotubes. According to EDX analysis, the ratio of metal to carbon was similar for Pt, Ru and Ti decorated samples but slightly lower for Cu and Ag however they all fall within an acceptable range for operational comparison, this may allow us to overlook the flake-like copper shapes for the purpose of this experiment. Also, the I_D/I_G ratio of the Raman results showed that the defects formed were due to the successful metal decoration and that they all are within the same range and ready for sensor fabrication and testing.

3.2. Sensor Response

The sensors were exposed to four pulses of the target gas in the sealed chamber. Upon each pulse, they exhibited a change in resistance in the form of a peak or a trough. An example is presented in **Figure 5** which shows the response of the Ru-MWCNT sensor to NO_2 gas and the remaining responses are presented in **Figure S1a -S1d** in the supporting document. The first pulse was neglected for stability issues and an average resistance change for each sensor was calculated using the remaining 3 pulses. The graph in **Figure 5** shows that the Ru-MWCNT sensor was able to recover to its baseline resistance and that its average resistance change upon NO_2 exposure was approximately 5.8 Ω. For each M-MWCNT sensor and for gas tested, the average change in resistance for the peaks is calculated and summarized in **Figure S2**. The response curves and average resistance change values of the 6 sensors to NO_2 **(Figure S1a and S2d)**, confirm that the sensors were more sensitive to NO_2 than the other gases. Some of the highest resistance changes for NO_2 were observed for the Ru, Pt and Ti-decorated MWCNTs which showed excellent recovery after gas exposure. The range of average resistance change for NO_2 detection is 1.6 to 5.8 Ω. On the other hand, all the sensors had very poor sensitivity to carbon monoxide **(Figure S1b and S2a)**, with observed change in resistance from 0.02 to 0.127 Ω, which is relatively minute with respect to the resistance changes of the other sensors. For H_2S **(Figure S1c)** and ammonia **(Figure S1d)**, the resistance change ranged from 0.58 to 3.80 Ω and from 0.98 to 3.15 Ω, respectively. The resistance

response graphs for ammonia shown in **Figure S1d** appear to have an increasing step-like feature for Pt and Ti decorated MWCNTs sensors, due to the insufficient time gap between gas pulses or that the desorption of the gas molecules in this case is more difficult to allow the sensor to recover back to its initial base resistance. The pristine carbon nanotubes-based sensor upon NH_3 exposure manages to avoid this issue. The direction of resistance change is caused by the potential of the target gases to act as reducing or oxidising gases when exposed to specific metal clusters, this will be discussed further in the Discussion section. However, during the programming of the sensor response, the direction is irrelevant because the absolute resistance change is used as the main indicator for the sensor programming.

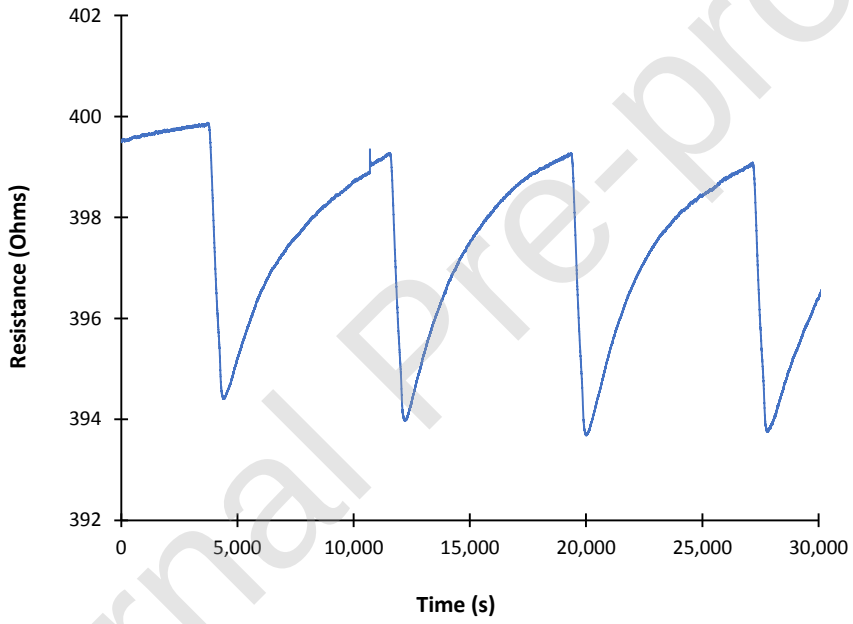

Figure 5: Response curve of Ru-MWCNT sensor to NO_2 gas measured at room temperature (20°C).

4. Discussion

4.1. Sensor Design

Each of the six sensors produced a response curve for their exposure to each of the 4 tested toxic gases, resulting in a total of 24 responses. Equation 1 was used to calculate the sensitivity (S) of each response based on the absolute difference in resistance of the sensor in synthetic air (R_{air}) and gas (R_{gas}).

The results in presented in **Table 2** and, graphically, in **Figure 6.a**. The initial R_{air} resistance values are labelled above each bar in **Figure 6.**

$$S = \frac{|R_{gas} - R_{air}|}{R_{air}} \, x \, 100. \qquad (1)$$

The CO response in **Figure 6a** was not clear with respect to the other gases, so we presented an expanded version of the CO response in **Figure 6b**. A simple binary pattern was implemented as an initial model such that it can be easily translated into future programming schematics. To determine the criteria upon which the response signal will be set to 0 or 1, we used the equation $S_{cutoff} = S_{max}/2$. For example, S_{max} (NH_3) = 0.944, thus S_{cutoff} = 0.944/2 = 0.472. Therefore, any response below 0.472 is set to 0 and any response higher and including S_{cutoff} will be set to 1. **Table 2** lists the preliminary identification pattern for each target gas using the metal-decorated carbon nanotube sensors presented in our work and the basis for building this sensor array.

Here, we have constructed a 6-sensor array that can generate a unique response pattern upon exposure for different toxic gases. While the degree of resistance change is important, the aim of this work was not to find the metal-decorated MWCNTs that will give the highest response, but rather the aim was to create this array that will generate a unique pattern to enable the identification of a target gas. This array can be used in the programming and development of the sensor to enable the simultaneous identification of multiple gases. There are different processing techniques such as the use of neural networks that allow the identification of the gas as well as the determination of the concentration.

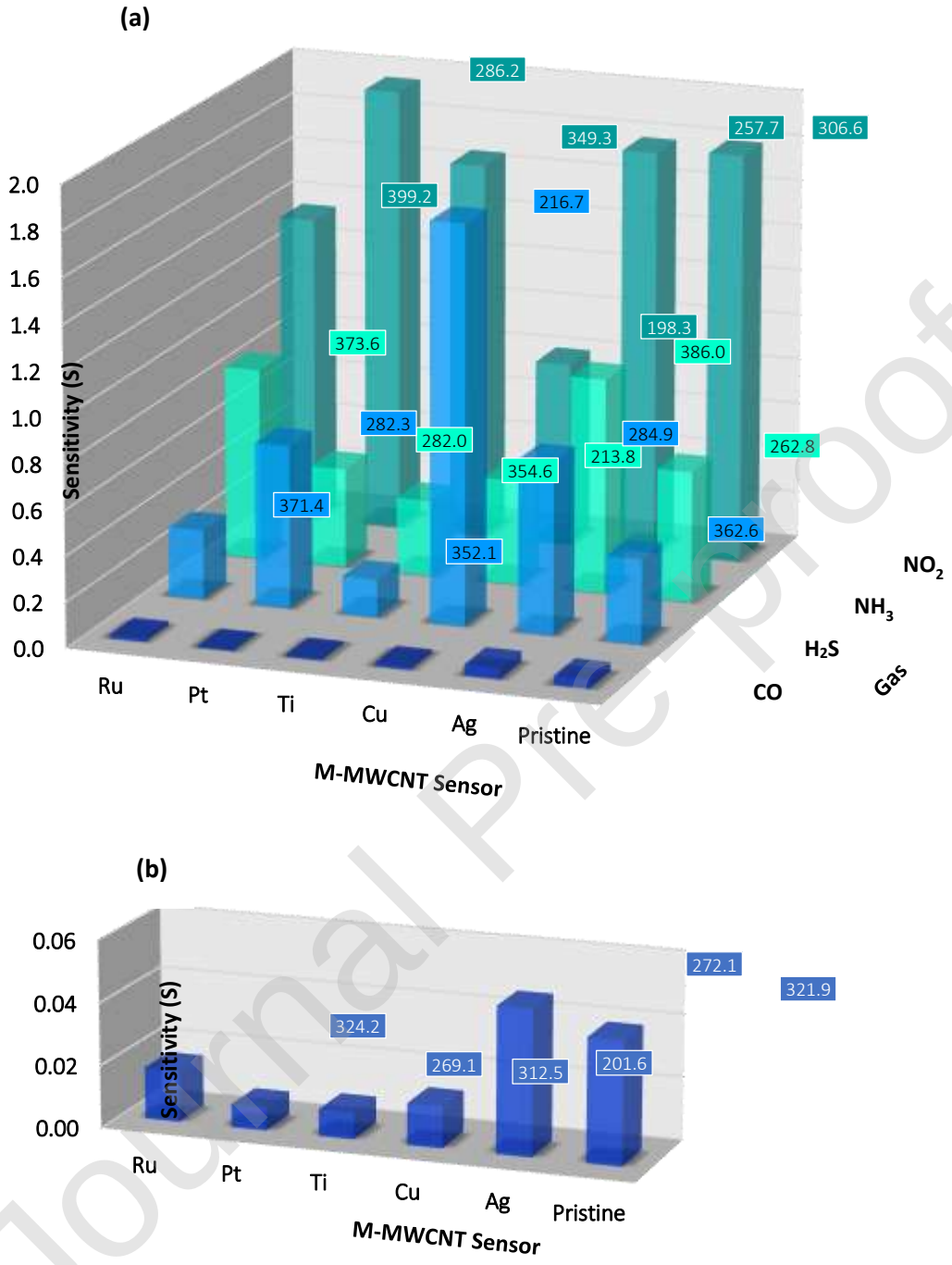

Figure 6: (a) Sensitivity of the M-MWCNTs and pristine MWCNTs sensors to CO, NO_2, NH_3 and H_2S and (b) Sensitivity of the M-MWCNT and pristine MWCNTs sensors to CO. Initial R_{air} at 20°C values (in Ω) are shown on each bar.

Table 2: Sensitivity response (S) of each M-MWCNTs and pristine MWCNTs to the target gases and Generated identifier patterns according to resistance change response

	CO (100 ppm)		**H_2S (10 ppm)**		**NH_3 (100 ppm)**		**NO_2 (10 ppm)**	
M-MWCNTs Sensor	**S**	**S_{cutoff} = 0.024**	**S**	**S_{cutoff} = 0.876**	**S**	**S_{cutoff} = 0.472**	**S**	**S_{cutoff} = 0.979**
Ru	0.016	0	0.305	0	0.843	1	1.353	1
Pt	0.007	0	0.714	0	0.437	0	1.957	1
Ti	0.009	0	0.166	0	0.334	0	1.660	1
Cu	0.013	0	1.752	1	0.460	0	0.807	0
Ag	0.047	1	0.755	0	0.944	1	1.783	1
Pristine	0.039	1	0.372	0	0.574	1	1.803	1
Identifier		**000011**		**000100**		**100011**		**111011**

Effect of Humidity

The relative humidity (RH) is a critical factor when designing the gas sensor because water molecules can impact the surface reactions between the active sensing material and the target gas. The resistance change of the fabricated sensors were tested in dry air, i.e. <10% RH (R_{10}) and the Ru-MWCNT, Ti-MWCNT and pristine MWCNT sensors were tested at ~50% RH (R_{50}) to NH_3 gas, to verify the ability of the sensors to operate at higher humidity, see **Table 3**. The humidity was tested using an SHT71 sensor placed in the outlet of the testing chamber. In the case of dry air, 100 ppm ammonia gas was diluted in an 80% N_2 and 20% O_2 commercial cylinder and fed directly into the sensor testing chamber. In the case of wet air testing using NH_3 gas, a Controlled Evaporation Mixing (CEM) system was used. CEM is a vapor generation system which consists of a liquid flow controller, an MFC for carrier gas and a temperature controlled mixing and evaporation device to generate humidity from a liquid source, in this case water, and mix it with the NH_3 dry air cylinder at 50:50 ratio as shown in **Figure S3** in the supporting information. The humidity remained stable at ~50% RH.

The sensors had a significant response to NH_3 gas in a 50% relative humid environment. The difference between the resistance changes at R_{10} and R_{50} ($\Delta R_{10/50}$) are calculated according to **Equation 2**. The average percentage difference, $\Delta R_{10/50}$, between the of the sensors in dry and wet air was calculated and presented in **Table 3** for each sensor and their average of the $\Delta R_{10/50}$ values was calculated to be 38%. The results verify the functionality of the sensors at higher humidity and the difference is attributed to the effect of humidity as well as other factors, such as lifetime/reusability of the sensor.

$$\Delta R_{10/50} = \frac{|R_{10} - R_{50}|}{R_{10}} \times 100 \qquad (2)$$

Table 3: Humidity comparison of Ru-MWCNTs, Ti-MWCNTs and Pristine MWCNT under NH_3 gas exposure. The values presented are the S values calculated according to Equation 1.

M-MWCNT Sensor	**Response of M-MWCNTs sensor to NH_3 under two cases of Relative Humidity (RH)**		
	Case 1: Dry Air (R_{10})	**Case 2: Wet Air (R_{50})**	**$\Delta R_{10/50}$**
Ru	0.843	1.256	48.99
Ti	0.334	0.422	26.35
Pristine	0.574	0.352	38.66

4.2. DFT Adsorption Mechanism and Comparison with Experimental Findings

The experimental results were compared to our previously reported DFT findings [28] to gain an atomic-level understanding of the gas-surface interactions and to compare and verify the DFT predictions of response. The DFT calculations investigated the effects of doping (8,0) SWCNTs, which acts as a p-type semiconductor, with Ti, Cu, and Pt metals and studied the change in the electronic properties upon exposure to NO_2 gas. Even though the inter-tube coupling of the multi-walled carbon nanotubes can affect the band structure, we chose to compare the multiwalled carbon nanotubes to the single walled DFT calculated carbon nanotubes because it was determined that the current flow only occurs through the outer most nanotube cylinder [34]. Moreover, the differences between doping and decorating are not well defined in literature, therefore the differences were neglected, and we focused on the similarities, where both methods create structural defects in the carbon nanotubes.

The diameter and chirality of carbon nanotubes determine their bandgap energy [35] and, consequently, whether they behave as semiconductors or metals [36]. The bandgap is approximately proportional to the inverse of the tube diameter [37]. Semiconducting carbon nanotubes are extremely sensitive to charge transfer and chemical doping effects by various molecules [24]. Upon exposure to electron-withdrawing molecules (e.g. NO_2, O_3, O_2) or electron-donating molecules (e.g. CO, H_2S, NH_3) [18], semiconducting carbon nanotubes behave as p-type semiconductors and change the resistance of the material by changing the density of the main charge carriers (holes) in the nanotubes [23,24,38]. Oxidizing gases (electron-withdrawing molecules) increase the density of holes thereby decreasing the resistance of the material, whereas reducing gases (electron-donating molecules) recombine the holes in the material with electrons thereby increasing the overall resistance of the material. Doping or decorating the carbon nanotubes' surface creates defects in the material, which give rise to interstitial surface states in the forbidden region. These surface states allow the presence of holes in the forbidden region, thereby decreasing the band gap width [39], which, in turn, increases the conductivity of the material as electrons from the valence band are excited to these new states leaving behind more holes for conduction. The charge transfer between the gas and surface is a redistribution of electrons around both surfaces [18]. The electrons are transferred to/from the HOMO and LUMO frontier orbitals of the gas and causes a narrowing/widening of the M-MWCNTs band gap, which changes the electrical conductivity of the material. DFT results from previous work [40] confirmed that upon exposure, the NO_2 molecule gained electrons from the total M-SWCNT complex due to the high electron affinity of NO_2 (2.3eV) [41] and that the equivalent gain in NO_2 charge is lost from the M-SWCNTs complex. NH_3, H_2S and CO, on the other hand, are reducing gases that donate electrons to the surface. When CO donates electrons, they refill the holes and decrease the conductivity. NH_3 and H_2S donate an excessive number of electrons causing the material to switch from p-type to n-type such that increase of electrons in the conduction band, in this case, leads to a decrease in resistance. Studies by Nguyen et al. [42] on the response of Co-MWCNTs and Zhang et al. who studied Pt-SWCNT's response to SO_2, H_2S and CO support out findings [17].

Our previous DFT calculations predicted that if the resistance of the M-doped SWCNTs is used as a selection baseline for the studied gas sensing materials, the highest increase in conductivity should be observed for Ti-SWCNTs followed by Pt-SWCNTs and then Cu-SWCNTs [28]. Ti transferred the highest number of electrons from the Ti-SWCNTs to the NO_2 gas molecule of 0.456 eV, followed by Pt-SWCNTs with Cu-SWCNTs having the lowest charge transfer of 0.351 eV. This is reflected in the change in bandgap. The band gap of pristine SWCNTs was 0.63 eV, the final band gap values of the M-SWCNTs when exposed to NO_2 are presented in **Table 4**. The doping of Ti and exposure to NO_2 created so many interstitial sites that the band gap disappeared, and the conductance and valence band experienced an overlap, given by the 0 eV band gap, giving the M-SWCNT metallic properties. Again, we see that the Pt doping follows Ti with Cu doping still maintaining the lowest charge transfer to NO_2 and largest band gap among the tested dopant metals. The smaller the band gap the easier for the current to be conducted, which makes the material more sensitive to resistance change. Comparing the DFT band gap values to the experimental average resistance change values of the M-MWCNTs sensors to NO_2 adsorption; Ti shows the highest average resistance increase (5.8 Ω), followed by Pt-MWCNTs (5.6 Ω), then Cu-MWCNTs (1.6 Ω) **(Table 4)**. The DFT calculations were successful in predicting the order of sensitivity of the different metal-carbon nanotubes combinations which validates the use of the DFT approach to simulate the particles to predict their experimental responses.

On an atomic-level, we find that the NO_2 band gap is formed between the $3\pi^*$ and $5\sigma^*$ levels. These are the levels that primarily take part in any NO_2 bonding to the M dopant, and therefore any electron donor to the NO_2 molecule will lead to the occupation of these levels [28]. For the interaction of CO, Zhang et al. ascribed the effect to the *p*-orbitals of C in CO to overlap with the *d*-orbitals of Pt, especially near the Fermi level and for H_2S adsorption on Pt-SWCNTs, they found that the *p*-orbitals of S have a large overlap with the *d*-orbitals of Pt, and that their strong interaction enhanced the adsorption between H_2S and the nanotube surface [42].

Table 4: Average resistance change per M-MWCNT for NO_2 exposure.

	Ti-SWCNT	**Pt-SWCNT**	**Cu-SWCNT**
Charge transferred from M-SWCNT to NO_2 Molecule (eV)	0.456	0.385	0.351
Band Gap (Eg) of M-SWCNT after NO_2 adsorption (eV)	0	0.104	0.183
Average resistance change response (Ω)	5.8	5.6	1.6

5. Conclusion and future perspective

Metal-decorated carbon nanotubes were synthesized using relatively simple lab techniques and characterized to indicate the successful formation of defects in the carbon nanotube wall caused by the attachment of metal clusters. The nanomaterial was deposited on gold-printed electrodes on Kapton sensors then upon exposure to four toxic gases. The degree to which the gas was adsorbed onto the M-MWCNTs differed from one metal to the other. The M-MWCNTs showed significant and unique responses that generated a pattern that can be used as an identifier for each gas. The results from this work are promising for the future development of sensitive and selective sensor arrays on metal-decorated MWCNTs for multiple industrial applications. The experimental results of the Ti, Pt, and Cu metal-decorated MWCNTs when exposed to NO_2 are in fact in the same order as predicted by DFT calculations, proving that DFT calculations can be used to predict the response of different materials as well as provide proof of concept, material screening and selection and comprehension of the adsorption mechanism.

This work provides the basis for other research areas to develop gas sensors based on metal-decorated carbon nanotubes. To generalize the concept, future work may investigate the percentage of metal cluster with respect to the carbon concentration. The percentage of metal in our active sensing powders was approximately 8-10%, higher percentages of metal maybe explored to investigate the effect of increasing the metal-to-carbon ratio on the response of the active layer and the sensitivity of the sensors. Moreover, testing of the resistance change of the sensor when it experiences a change in gas concentration could be another point of interest.

Author Statement

Icell Sharafeldin: Data curation; Formal analysis; Investigation; Methodology; Validation; Visualization; Writing - original draft; Writing - review & editing.

Sara Garcia-Rios: Formal analysis; Investigation; Methodology; Validation; Visualization.

Nashaat Ahmed: Formal analysis; Investigation; Methodology; Validation; Visualization; Writing - original draft.

Miriam Alvarado: Formal analysis; Investigation; Methodology; Validation; Visualization.

Xavier Vilanova: Investigation; Resources; Supervision; Writing - original draft; Writing - review & editing.

Nageh K. Allam: Conceptualization; Formal analysis; Funding acquisition; Project administration; Resources; Supervision; Visualization; Writing - original draft; Writing - review & editing.

Declaration of interests

The authors declare that they have no known competing financial interests or personal relationships that could have appeared to influence the work reported in this paper.

References

[1] MarketsandMarkets™, Gas Sensors Market Size, Share, system and Industry Analysis and Market Forecast to 2024, (2019). https://www.marketsandmarkets.com/Market-Reports/gas-sensor-market-245141093.html (accessed March 12, 2020).

[2] B. Hoffheins, Solid state, resistive gas sensors, in: R.F. Taylor, J.S. Schultz (Eds.), Handb. Chem. Biol. Sensors, Institute of Physics, Bristol and Philadelphia, 1996.

[3] S. Hooker, Nanotechnology advantages applied to gas sensor development, in: Proc. 5th Annu. BCC Nanoparticles, 2002: pp. 1–7. http://www.boulder.nist.gov/div853/Publicationfiles/NIST_BCC_Nano_Hooker_2002.pdf

[4] Y. Hong, C.-H. Kim, J. Shin, K.Y. Kim, J.S. Kim, C.S. Hwang, J.-H. Lee, Highly selective ZnO gas sensor based on MOSFET having a horizontal floating-gate, Sensors Actuators B Chem. 232 (2016) 653–659. https://doi.org/10.1016/J.SNB.2016.04.010.

[5] S. Zhu, Y. Liu, G. Wu, L. Fei, S. Zhang, Y. Hu, Z. Yan, Y. Wang, H. Gu, W. Chen, Mechanism study on extraordinary room-temperature CO sensing capabilities of Pd-SnO2 composite nanoceramics, Sensors Actuators B Chem. 285 (2019) 49–55. https://doi.org/10.1016/j.snb.2019.01.027.

[6] N.O. Guldal, H.E. Figen, S.Z. Baykara, New catalysts for hydrogen production from H 2 S: Preliminary results, Int. J. Hydrogen Energy. 40 (2015) 7452–7458. https://doi.org/10.1016/j.ijhydene.2015.02.107.

[7] L.E. Kreno, J.T. Hupp, R.P. Van Duyne, Metal−Organic Framework Thin Film for Enhanced Localized Surface Plasmon Resonance Gas Sensing, Anal. Chem. 82 (2010) 8042–8046. https://doi.org/10.1021/ac102127p.

[8] F. Qu, H. Jiang, M. Yang, Designed formation through a metal organic framework route of ZnO/$ZnCo_2O_4$ hollow core–shell nanocages with enhanced gas sensing properties, Nanoscale. 8 (2016) 16349–16356. https://doi.org/10.1039/C6NR05187A.

[9] H. Bai, G. Shi, Gas Sensors Based on Conducting Polymers, Sensors (Basel). 7 (2007) 267–307. https://www.ncbi.nlm.nih.gov/pmc/articles/PMC3756721/.

[10] E. Llobet, Gas sensors using carbon nanomaterials: A review, Sensors Actuators B. Chem. 179 (2012) 32-45. https://doi.org/10.1016/j.snb.2012.11.014.

[11] D. Raeyani, S. Shojaei, S. Ahmadi-Kandjani, Optical graphene quantum dots gas sensors: experimental study, Mater. Res. Express. 7 (2020) 015608. https://doi.org/10.1088/2053-1591/ab637e.

[12] B. Jiang, Y. Guo, J. Kim, A.E. Whitten, K. Wood, K. Kani, A.E. Rowan, J. Henzie, Y. Yamauchi, Mesoporous Metallic Iridium Nanosheets, J. Am. Chem. Soc. 140 (2018) 12434–12441.

https://doi.org/10.1021/jacs.8b05206.

[13] Y. Li, J. Pionteck, P. Pötschke, B. Voit, Thermal annealing to influence the vapor sensing behavior of co-continuous poly(lactic acid)/polystyrene/multiwalled carbon nanotube composites, Mater. Des. 187 (2020) 108383. https://doi.org/10.1016/j.matdes.2019.108383.

[14] C. Li, M. Iqbal, J. Lin, X. Luo, B. Jiang, V. Malgras, K.C.W. Wu, J. Kim, Y. Yamauchi, Electrochemical Deposition: An Advanced Approach for Templated Synthesis of Nanoporous Metal Architectures, Acc. Chem. Res. 51 (2018) 1764–1773. https://doi.org/10.1021/acs.accounts.8b00119.

[15] C. Li, M. Iqbal, B. Jiang, Z. Wang, J. Kim, A.K. Nanjundan, A.E. Whitten, K. Wood, Y. Yamauchi, Pore-tuning to boost the electrocatalytic activity of polymeric micelle-templated mesoporous Pd nanoparticles, Chem. Sci. 10 (2019) 4054–4061. https://doi.org/10.1039/C8SC03911A.

[16] J. Casanova-Cháfer, È. Navarrete, E. Llobet, Gas Sensing Properties of Carbon Nanotubes Decorated with Iridium Oxide Nanoparticles, Proceedings. 2 (2018) 874. https://doi.org/10.3390/proceedings2130874.

[17] M. A. Mohamed, A. M. Yehia, C. E. Banks, N. K. Allam, Novel MWCNTs/graphene oxide/pyrogallol composite with enhanced sensitivity for biosensing applications, Biosensors and Bioelectronics 89 (2017) 1034-1041. https://doi.org/10.1016/j.bios.2016.10.025.

[18] K. Li, W. Wang, D. Cao, Metal (Pd, Pt)-decorated carbon nanotubes for CO and NO sensing, Sensors Actuators B Chem. 159 (2011) 171–177. https://doi.org/10.1016/j.snb.2011.06.068.

[19] C. Li, H. Tan, J. Lin, X. Luo, S. Wang, J. You, Y.-M. Kang, Y. Bando, Y. Yamauchi, J. Kim, Emerging Pt-based electrocatalysts with highly open nanoarchitectures for boosting oxygen reduction reaction, Nano Today. 21 (2018) 91–105. https://doi.org/10.1016/j.nantod.2018.06.005.

[20] C. Verissimo, M. Ding, A. Abbaspourrad, A. Star, S. Moshkalev, Decorated Single- and Multi-Walled Carbon Nanotubes Aiming H_2S sensing, TechConnect Briefs. 1, Nanotech (2011) 181–184.

[21] M. Angjellari, E. Tamburri, G. Reina, M. Tomellini, M.L. Terranova, T.C. Minimalab, R. Tor, V. Della Ricerca, M. Pasquali, Coupling of nickel nanoparticles with carbon nanotubes fibers : a new concept towards multifunctional devices, in: IEE Int. Conf. Nanotechnol., 2015: pp. 1074–1077.

[22] E. Espinosa, R. Ionescu, B. Chambon, G. Bedis, E. Sotter, C. Bittencourt, A. Felten, J. Pireaux, X. Correig, E. Llobet, Hybrid metal oxide and multiwall carbon nanotube films for low temperature gas sensing, Sensors Actuators B Chem. 127 (2007) 137–142. https://doi.org/10.1016/j.snb.2007.07.108.

[23] M. Penza, G. Cassano, R. Rossi, M. Alvisi, A. Rizzo, M.A. Signore, T. Dikonimos, E. Serra, R.

Giorgi, Enhancement of sensitivity in gas chemiresistors based on carbon nanotube surface functionalized with noble metal (Au, Pt) nanoclusters, Appl. Phys. Lett. 90 (2007) 173123. https://doi.org/10.1063/1.2722207.

[24] E. Dilonardo, M. Penza, M. Alvisi, C. Di Franco, R. Rossi, F. Palmisano, L. Torsi, N. Cioffi, Electrophoretic deposition of Au NPs on MWCNT-based gas sensor for tailored gas detection with enhanced sensing properties, Sensors Actuators B Chem. 223 (2016) 417–428. https://doi.org/10.1016/j.snb.2015.09.112.

[25] A. Star, V. Joshi, S. Skarupo, D. Thomas, J.-C.P. Gabriel, Gas Sensor Array Based on Metal-Decorated Carbon Nanotubes, J. Phys. Chem. B. 110 (2006) 21014–21020. https://doi.org/10.1021/jp064371z.

[26] N. Ahmed, M. Ramadan, W. M. A. El Rouby, A. A. Farghali, N. K. Allam, Non-precious co-catalysts boost the performance of TiO_2 hierarchical hollow mesoporous spheres in solar fuel cells, Int. J. Hydrogen Energy 43 (2018) 21219-21230. https://doi.org/10.1016/j.ijhydene.2018.10.012.

[27] Y. Wang, R. Zhang, J. Li, L. Li, S. Lin, First-principles study on transition metal-doped anatase TiO_2, Nanoscale Res. Lett. 9 (2014) 46. https://doi.org/10.1186/1556-276X-9-46.

[28] I.M. Sharafeldin, N.K. Allam, DFT insights into the electronic properties and adsorption of NO_2 on metal-doped carbon nanotubes for gas sensing applications, New J. Chem. 41 (2017) 14936–14944. https://doi.org/10.1039/C7NJ03109B.

[29] M. Baro, P. Nayak, T.T. Baby, S. Ramaprabhu, Green approach for the large-scale synthesis of metal/metal oxidenanoparticle decorated multiwalled carbon nanotubes, J. Mater. Chem. A. 1 (2013) 482–486. https://doi.org/10.1039/C2TA00483F.

[30] A.D. Dobrzańska-Danikiewicz, D. Łukowiec, D. Cichocki, W. Wolany, Carbon nanotubes manufacturing using the CVD equipment against the background of other methods, Arch. Mater. Sci. Eng. 64 (2013) 103–109.

[31] R. Scaffaro, A. Maio, S. Agnello, A. Glisenti, Plasma Functionalization of Multiwalled Carbon Nanotubes and Their Use in the Preparation of Nylon 6-Based Nanohybrids, Plasma Process. Polym. 9 (2012) 503–512. https://doi.org/10.1002/ppap.201100140.

[32] E.F. Antunes, V.G. de Resende, U.A. Mengui, J.B.M. Cunha, E.J. Corat, M. Massi, Analyses of residual iron in carbon nanotubes produced by camphor/ferrocene pyrolysis and purified by high temperature annealing, Appl. Surf. Sci. 257 (2011) 8038–8043. https://doi.org/10.1016/j.apsusc.2011.04.090.

[33] B. A. Ali, O. I. Metwalli, A. S. G. Khalil, N. K. Allam, Unveiling the Effect of the Structure of Carbon Material on the Charge Storage Mechanism in MoS_2-Based Supercapacitors, ACS omega 3 (2018) 16301-16308. https://doi.org/10.1021/acsomega.8b02261

[34] P.R. Bandaru, Electrical Properties and Applications of Carbon Nanotube Structures, J. Nanosci. Nanotechnol. 7 (2007) 1239–1267. https://doi.org/10.1166/jnn.2007.307.

[35] M. Ouyang, Energy Gaps in "Metallic" Single-Walled Carbon Nanotubes, Science 292 (2001) 702–705. https://doi.org/10.1126/science.1058853.

[36] A. Aqel, K.M.M.A. El-Nour, R.A.A. Ammar, A. Al-Warthan, Carbon nanotubes, science and technology part (I) structure, synthesis and characterisation, Arab. J. Chem. 5 (2012) 1–23. https://doi.org/10.1016/j.arabjc.2010.08.022.

[37] X. Liu, T. Pichler, M. Knupfer, M.S. Golden, J. Fink, H. Kataura, Y. Achiba, Detailed analysis of the mean diameter and diameter distribution of single-wall carbon nanotubes from their optical response, Phys. Rev. B. 66 (2002) 045411. https://doi.org/10.1103/PhysRevB.66.045411.

[38] S. Mao, G. Lu, J. Chen, Nanocarbon-based gas sensors: progress and challenges, J. Mater. Chem. A. 2 (2014) 5573. https://doi.org/10.1039/c3ta13823b.

[39] S. George, S. Pokhrel, Z. Ji, B.L. Henderson, T. Xia, L. Li, J.I. Zink, A.E. Nel, L. Mädler, Role of Fe Doping in Tuning the Band Gap of TiO_2 for the Photo-Oxidation-Induced Cytotoxicity Paradigm, J. Am. Chem. Soc. 133 (2011) 11270–11278. https://doi.org/10.1021/ja202836s.

[40] I.M. Sharafeldin, N.K. Allam, DFT insights into the electronic properties and adsorption of NO_2 on metal-doped carbon nanotubes for gas sensing applications, New J. Chem. 41 (2017) 14936–14944. https://doi.org/10.1039/C7NJ03109B.

[41] K.M. Ervin, J. Ho, W.C. Lineberger, Ultraviolet photoelectron spectrum of nitrite anion, J. Phys. Chem. 92 (1988) 5405–5412. https://doi.org/10.1021/j100330a017.

[42] X. Zhang, Z. Dai, L. Wei, N. Liang, X. Wu, Theoretical Calculation of the Gas-Sensing Properties of Pt-Decorated Carbon Nanotubes, Sensors. 13 (2013) 15159–15171. https://doi.org/10.3390/s131115159.